Multimode Carrier-Based PWM Strategy of Open-End Winding PMSM With Isolated DC Sources

Xin Gu, *Member, IEEE*, Yufei Liu, *Student Member, IEEE*, Guozheng Zhang, *Member, IEEE*, Yanfei Cao, *Member, IEEE*, and Changliang Xia, *Senior Member, IEEE*

***Abstract*—A multimode carrier-based PWM strategy for open-end winding permanent-magnet synchronous motor (OW-PMSM) with isolated dc sources is proposed in this article. For the proposed strategy, the independent reference voltages of both the two inverters are obtained by decomposing the reference voltage output from the controller. Then, multiple modulation modes are established by different combinations of continuous PWM, discontinuous PWM and duty-cycle modulation for dual-inverter. As a result, the switching times of dual-inverter in each carrier period can be varied from 6 to 2. For the proposed strategy, the reference voltage is always synthesized by the nearest switching states. Thus, the output waveform quality for dual-inverter of the proposed strategy is better than that of the traditional modulation strategies. The feasibility and effectiveness of the proposed multimode modulation strategy is experimentally validated using a 4.3-kW OW-PMSM prototype.**

***Index Terms*—DC–AC inverter, harmonic distortion, permanent magnet motors, puleswidth modulation (PWM).**

I. Introduction

THE dual-inverter fed open-end winding permanent-magnet synchronous motor system has the advantages of low harmonic distortion, high dc-link voltage utilization and good fault tolerance [1]. Compared with the neutral-point-clamped three-level inverter, the number of output voltage levels of dual-inverter are the same. And there is no need to control the neutral-point voltage [2]. Thus, dual-inverter fed open-end winding permanent-magnet synchronous motor (OW-PMSM) can be widely used in high-power medium-voltage applications, such as locomotive traction [3], ship propulsion [4], and starter generator [5].

According to the topology of dc source, dual-inverter fed OW-PMSM system can be categorized into three types.

1) Common dc source.
2) Single dc source with a floating capacitor bridge.
3) Dual isolated dc sources.

Zero sequence current (ZSC) are generated in the common dc sources topology due to the existence of zero sequence loops. Hence, the output performance of the dual-inverter will be affected [6]. The single dc source with a floating capacitor bridge topology requires additional control of the floating capacitor voltage [7]. It has lower voltage utilization then the common dc sources topology [8]. For the dual isolated dc sources topology, the effect of ZSC on the system does not need to be considered because there is no zero sequence loop. Thus, the output performance and operation efficiency can be improved compare with other two topologies.

Modulation strategies of OW-PMSM can be mainly categorized into carrier-based PWM (CBPWM) [4] and space-vector PWM [9]. CBPWM has been widely studied due to its simple easy digital implementation. For the common dc source topology, the research topic mainly focuses on reducing the ZSC. A CBPWM method which ensures that the average value of ZSC in each carrier period is zero is proposed in [10]. There are two switching actions for each phase of dual-inverter in every carrier period. On this basis, a ZSC suppression method is proposed in [11]. There is only one switching action for each phase in every carrier period. Meanwhile, the common-mode voltage of dual-inverter is also kept to zero. The switching loss can be further reduced by the method proposed in [12]. There are two phases without switching actions in each carrier period. And the ZSC can still be restrained. Moreover, the maximum modulation range of the proposed method for OW-PMSM system is also analyzed. For the single dc source with a floating capacitor bridge topology, the research topic mainly focuses on the floating capacitor voltage control. In [13], the floating capacitor voltage is controlled by adjusting the angle between the reference voltages of the two inverters. In [14], an improved floating capacitor voltage control algorithm is proposed. And the volume of the capacitor could be reduced. The output harmonic distortion of dual-inverter under different ratio of dc source voltage to floating capacitor voltage is analyzed and the optimal ratio is determined [15].

For dual isolated dc sources topology, the research topic mainly focuses on improving the output performance and efficiency of dual-inverter. In [16], zero vectors are not adopted, and there are two legs without switching actions in each carrier period. The decoupling angle between the reference voltages of the

Received 22 May 2024; revised 21 September 2024; accepted 2 October 2024. Date of publication 7 October 2024; date of current version 12 December 2024. This work was supported in part by the National Key Research and Development Program of China under Grant 2022YFB2502803 and in part by the National Natural Science Foundation of China under Grant 52177055. Recommended for publication by Associate Editor B. Singh. *(Corresponding author: Guozheng Zhang.)*

Xin Gu and Guozheng Zhang are with the School of Electrical Engineering, Tiangong University, Tianjin 300387, China (e-mail: guxin@tiangong.edu.cn; zhanggz@tju.edu.cn).

Yufei Liu is with the School of Control Science and Engineering, Tiangong University, Tianjin 300387, China (e-mail: liuyufei@tiangong.edu.cn).

Yanfei Cao and Changliang Xia are with the College of Electrical Engineering, Zhejiang University, Hangzhou 310027, China (e-mail: caoyanfei@zju.edu.cn; motor@tju.edu.cn).

Color versions of one or more figures in this article are available at https://doi.org/10.1109/TPEL.2024.3475475.

Digital Object Identifier 10.1109/TPEL.2024.3475475

two inverters is modified to ensure the operation of OW-PMSM and the harmonic distortion of the output current is reduced. A minimum switching action modulation method is proposed in [17]. There are four legs without switching actions in each carrier period and the switching loss can be further reduced. Similarly, four PWM schemes simultaneously clamps two phases of each inverter throughout the fundamental period are proposed in [18]. The switching transition in the pole voltage can be reduced. In [19], the dwell time of zero vector is redistributed to realize the balanced control of the switching loss between the two inverters. For all the mentioned modulation methods, reference voltages of the two inverters are calculated separately. Then, the two inverters are modulated independently. In [20], reference voltage is assigned to dual-inverter by a certain pattern. The reference voltage is always synthesized by the nearest switching states. Thus, the output waveform quality of dual-inverter is improved. A discontinuous PWM (DPWM) method with reference voltage decomposition is proposed in [21]. The mathematical relationship between the clamping interval and the switching loss is calculated and then the optimal clamping mode is obtained by the genetic algorithm. A DPWM method with four output voltage level is proposed in [22]. The switching loss and the harmonic distortion can be reduced simultaneously. The current ripple of an OW-PMSM with the adoption of decoupled DPWM is analytically expressed in [23]. The harmonic distortion of the output current is reduced by unsymmetrical distribution of the dwell time of zero vector in each carrier period. For all the mentioned DPWM methods, the switching loss of dual-inverter is suppressed by the specific distribution of clamping intervals. However, the switching loss can be further reduced by the appropriate design of reference voltage and the different combination of modulation methods for dual-inverter. In [24], various modulation methods with different number of switching actions in each carrier period are proposed. The operation of OW-PMSM in the wide speed range can be realized. In this article, the redundant switching states of dual-inverter are fully utilized by designing the independent reference voltages of the two inverters. Then, a multimode CBPWM is proposed to reduce the switching loss in the full modulation range. Meanwhile, reference voltages for different modulation modes are always synthesized by the nearest switching states. Therefore, the output waveform quality of dual-inverter is improved simultaneously. In recent years, topologies of dual-inverter fed OW-PMSM with fuel cell-battery or two batteries are proposed in [25] and [26], which shows the wide application prospect of the OW-PMSM with dual isolated dc sources in electric vehicles.

The rest this article is organized as follows. The topology of the dual-inverter fed OW-PMSM with isolated dc sources is introduced in Section II. The principle of the proposed multimode CBPWM strategy is presented in Section III. Expressions of reference voltage for dual-inverter in different modulation mode are given. In Section IV, the experimental prototype of dual-inverter fed OW-PMSM is established and the output performance of the proposed CBPWM strategy is experimental analyzed. The innovation and the advantage of the proposed strategy are summarized in Section V.

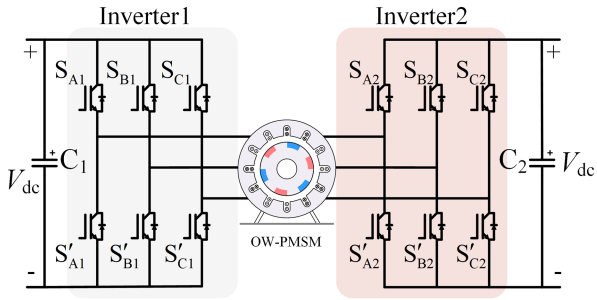

Fig. 1. Topology of dual-inverter fed OW-PMSM with isolated DC sources.

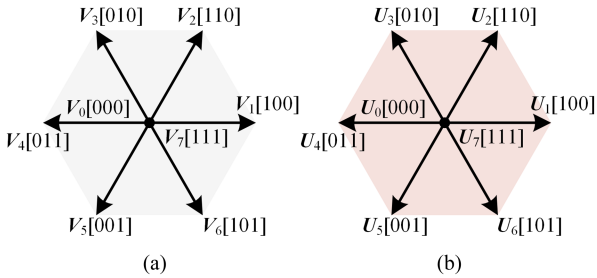

Fig. 2. Space vector diagram of inverter 1 and inverter 2. (a) Inverter 1. (b) Inverter 2.

II. Topology of OW-PMSM With Isolated DC Sources

The topology of dual-inverter fed OW-PMSM with dual isolated dc sources is shown in Fig. 1. The two-level inverter on each side of OW-PMSM is supplied by an isolated dc source. For each inverter, there are eight switching states corresponding to eight basic voltage vectors in the space vector diagram, as shown in Fig. 2. "1" represents the switching state of the power switch in the upper leg is ON and the switching state of the power switch in the lower leg is OFF. While, "0" represents the switching state of the power switch in the upper leg is OFF and the switching state of the power switch in the lower leg is ON. $\boldsymbol{V}_i$ ($i = 0, 1, 2, \ldots, 7$) represents the basic vector of inverter 1 and $\boldsymbol{U}_n$ ($n = 0, 1, 2, \ldots, 7$) represents the basic vector of inverter 2. For dual-inverter, there are $8^2 = 64$ switching states corresponding to 64 basic vectors in the space vector diagram, as shown in Fig. 3. The space vector diagram can be divided into six sectors $Z_I \sim Z_{VI}$, and each sector can be further divided into six regions 1–6. The basic voltage vector is defined as ***i-n***. And the basic vectors which occupies in the same place are defined as redundant vectors.

The relationship between the reference vector $\boldsymbol{V}_{\mathrm{ref}}$ of dual-inverter and reference vectors $\boldsymbol{V}_{\mathrm{ref1}}$ and $\boldsymbol{V}_{\mathrm{ref2}}$ of the two individual inverters is

$$\boldsymbol{V}_{\mathrm{ref}} = \boldsymbol{V}_{\mathrm{ref1}} - \boldsymbol{V}_{\mathrm{ref2}}. \tag{1}$$

The modulation index m is defined as

$$m = \frac{\sqrt{3}V_{\mathrm{ref}}}{2V_{\mathrm{dc}}} \tag{2}$$

where V_{ref} is the amplitude of the reference voltage and V_{dc} is the voltage of dc sources.

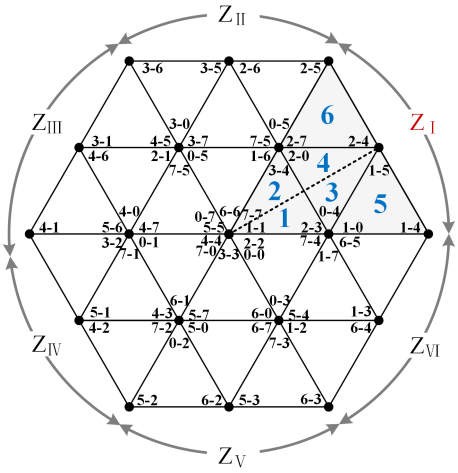

Fig. 3. Space vector diagram of dual-inverter.

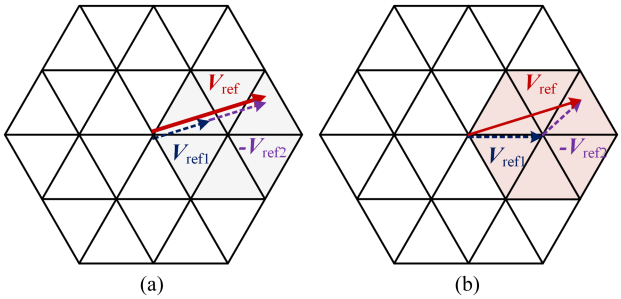

Fig. 4. Traditional modulation method of dual-inverter. (a) 180° decoupled modulation. (b) Clamped modulation.

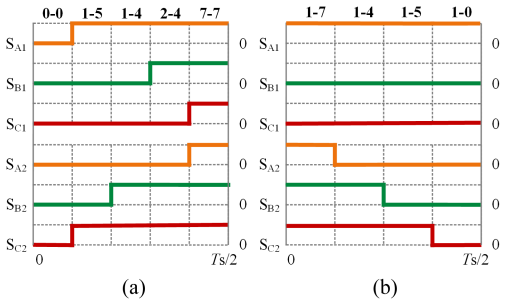

Fig. 5. Switching sequence in the first half of the carrier period. (a) 180° decoupled modulation. (b) Clamped modulation.

The traditional modulation methods of dual-inverter fed OW-PMSM can be divided into two types: 180° decoupled modulation and clamped modulation. For 180° decoupled modulation, amplitudes of $\boldsymbol{V}_{\mathrm{ref1}}$ and $\boldsymbol{V}_{\mathrm{ref2}}$ are the same and the directions of $\boldsymbol{V}_{\mathrm{ref1}}$ and $\boldsymbol{V}_{\mathrm{ref2}}$ are opposite, as shown in Fig. 4(a). For clamped modulation, $\boldsymbol{V}_{\mathrm{ref1}}$ can be any non-zero basic vector and then $\boldsymbol{V}_{\mathrm{ref2}}$ is obtained according to the principle of vector synthesis, as shown in Fig. 4(b). Switching sequences in the first half carrier period of the above two modulation methods are shown in Fig. 5.

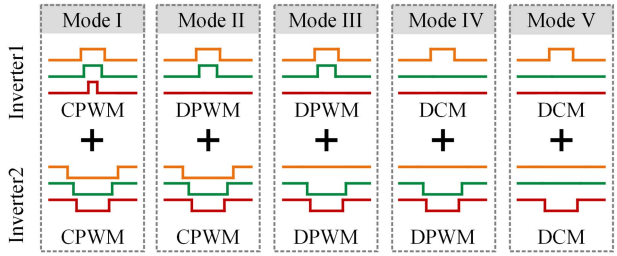

Fig. 6. Combinations of different modulation methods for dual-inverter corresponding to modes I–V.

For 180° decoupled modulation, both inverters 1 and 2 adopt continuous PWM (CPWM). There are six switching actions in each carrier period for dual-inverter, as shown in Fig. 5(a). For clamped modulation, $\boldsymbol{V}_{\mathrm{ref1}}$ can only be nonzero basic vectors, so that there is no switching action for inverter 1 in each carrier period. Meanwhile, inverter 2 adopts CPWM. Thus, there are three switching actions in each carrier period for dual-inverter, as shown in Fig. 5(b).

III. Multimode Carrier-Based PWM Strategy

For OW-PMSM, CPWM, DPWM, and duty-cycle modulation (DCM) can be used by inverters 1 and 2 independently. Then, different modulation modes with the number of switching actions varies from 6 to 2 in each carrier period for dual-inverter can be established, as shown in Fig. 6. Five different modulation modes are defined as follow: For mode I, inverters 1 and 2 both adopt CPWM and there are six switching actions in each carrier period. For mode II, inverter 1 adopts DPWM and inverter 2 uses CPWM. There are five switching actions in each carrier period. For mode III, inverters 1 and 2 both adopt DPWM and there are four switching actions in each carrier period. For mode IV, inverter 1 adopts DCM and inverter 2 uses DPWM. There are three switching actions in each carrier period. For mode V, inverters 1 and 2 both adopt DCM and there are two switching actions in each carrier period.

The reference voltage of dual-inverter can be expressed as $v{*}x = v_x + v_{\mathrm{z}}, x \in \{\mathrm{A}, \mathrm{B}, \mathrm{C}\}$. Where, v_x is the sinusoidal voltage and v_{z} is the zero-sequence voltage. For modes I–V, $\boldsymbol{V}_{\mathrm{ref}}$ is always synthesized by the three nearest basic vectors. Taking region 1 of sector Z_{I} as an example, the computation of reference voltages v_{x1} and v_{x2} for inverters 1 and 2 are shown as follow.

In Fig. 7(a), both inverters 1 and 2 adopt CPWM for mode I. In the first half carrier period, the switching sequence of Inverter 1 is $\boldsymbol{V}_0 \rightarrow \boldsymbol{V}_1 \rightarrow \boldsymbol{V}_2 \rightarrow \boldsymbol{V}_7$ and the switching sequence of Inverter 2 is $\boldsymbol{U}_7 \rightarrow \boldsymbol{U}_4 \rightarrow \boldsymbol{U}_5 \rightarrow \boldsymbol{U}_0$. Then, the synthesized switching sequence of dual-inverter can be expressed as **0-7** →**0-4**→**0-5**→**0-0**→**1-0**→**2-0**→**7-0**. Based on the principle of volt-second balance and the geometrical relations in Fig. 7(a), the dwell time T_0, T_1, and T_2 of basic vectors (including redundant vectors) are as follows:

$$\begin{cases} T_0 = T_{\mathrm{s}}\left[1 + (v_{\min} - v_{\max})/(V_{\mathrm{dc}}/2)\right] \\ T_1 = T_{\mathrm{s}}(v_{\max} - v_{\mathrm{mid}})/(V_{\mathrm{dc}}/2) \\ T_2 = T_{\mathrm{s}}(v_{\mathrm{mid}} - v_{\min})/(V_{\mathrm{dc}}/2) \end{cases} \tag{3}$$

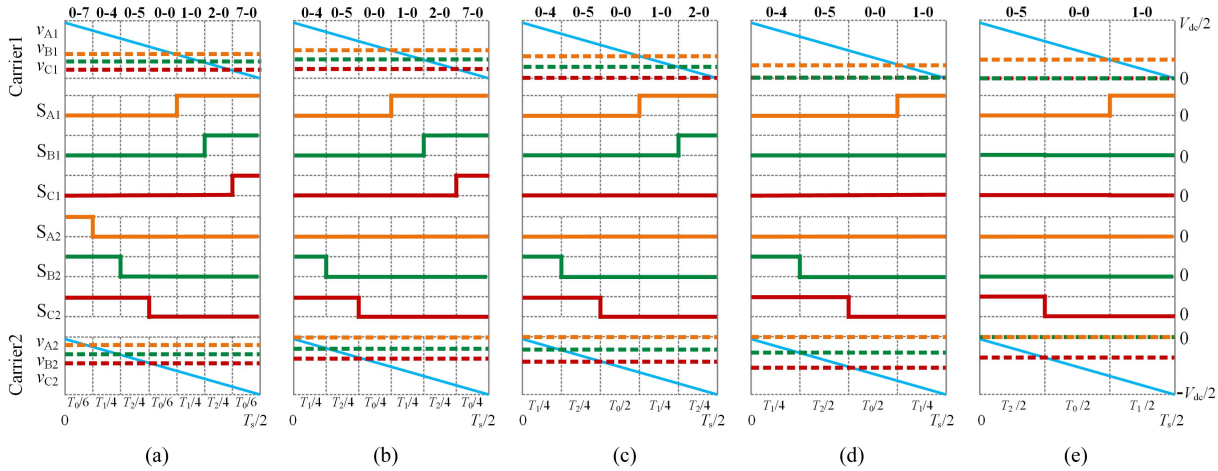

Fig. 7. Switching sequence of dual-inverter with the adoption of different modes in region 1 of sector Z_I. (a) Mode I. (b) Mode II. (c) Mode III. (d) Mode IV. (e) Mode V.

TABLE I
EXPRESSION OF REFERENCE VOLTAGE FOR EACH MODULATION MODE IN SECTOR Z_I

Mode	Region	Carrier1	Carrier2	Reference Voltage		
Mode I	1	0	0	$v_{A1}=v_{max}/6-v_{min}/6+V_{dc}/6$ $v_{A2}=v_{max}/3-v_{min}/3-V_{dc}/6$	$v_{B1}=-v_{max}/3+v_{mid}/2-v_{min}/6+V_{dc}/6$ $v_{B2}=-v_{max}/6+v_{mid}/2-v_{min}/3-V_{dc}/6$	$v_{C1}=-v_{max}/3+v_{min}/3+V_{dc}/6$ $v_{C2}=-v_{max}/6+v_{min}/3-V_{dc}/6$
Mode II	1	0	0	$v_{A1}=V_{dc}/4$ $v_{A2}=0$	$v_{B1}=-v_{max}/2+v_{mid}/2+V_{dc}/4$ $v_{B2}=-v_{max}/2+v_{mid}/2$	$v_{C1}=-v_{max}/2+v_{min}/2+V_{dc}/4$ $v_{C2}=-v_{max}/2+v_{min}/2$
Mode III	1	0	0	$v_{A1}=v_{max}/2-v_{min}/2$ $v_{A2}=0$	$v_{B1}=v_{mid}/2-v_{min}/2$ $v_{B2}=-v_{max}/2+v_{mid}/2$	$v_{C1}=0$ $v_{C2}=-v_{max}/2+v_{min}/2$
	3	0	0	$v_{A1}=v_{max}/2-v_{min}/2$ $v_{A2}=0$	$v_{B1}=-v_{max}/2+v_{mid}/2+V_{dc}/4$ $v_{B2}=v_{mid}/2-v_{min}/2-V_{dc}/4$	$v_{C1}=0$ $v_{C2}=-v_{max}/2+v_{min}/2$
	5	0	π	$v_{A1}=V_{dc}/2$ $v_{A2}=0$	$v_{B1}=v_{mid}/2+V_{dc}/4$ $v_{B2}=v_{mid}/2-V_{dc}/4$	$v_{C1}=v_{min}/2+V_{dc}/4$ $v_{C2}=v_{min}/2-V_{dc}/4$
Mode IV	1	0	0	$v_{A1}=v_{max}/2-v_{mid}/2$ $v_{A2}=0$	$v_{B1}=0$ $v_{B2}=-v_{max}/2+v_{mid}/2$	$v_{C1}=0$ $v_{C2}=-v_{max}/2-v_{mid}/2+v_{min}$
	3	0	0	$v_{A1}=v_{max}-v_{mid}/2-v_{min}/2-V_{dc}/4$ $v_{A2}=0$	$v_{B1}=0$ $v_{B2}=v_{mid}/2-v_{min}/2-V_{dc}/4$	$v_{C1}=0$ $v_{C2}=-v_{mid}/2+v_{min}/2-V_{dc}/4$
	5	0	0	$v_{A1}=v_{max}/2-v_{min}/2$ $v_{A2}=0$	$v_{B1}=0$ $v_{B2}=-v_{max}/2+v_{mid}-v_{min}/2$	$v_{C1}=0$ $v_{C2}=-v_{max}/2+v_{min}/2$
Mode V	1	0	0	$v_{A1}=v_{max}-v_{mid}$ $v_{A2}=0$	$v_{B1}=0$ $v_{B2}=0$	$v_{C1}=0$ $v_{C2}=-v_{mid}+v_{min}$
	3	0	0	$v_{A1}=v_{max}$ $v_{A2}=0$	$v_{B1}=0$ $v_{B2}=v_{mid}$	$v_{C1}=0$ $v_{C2}=-V_{dc}/2$
	5	0	0	$v_{A1}=v_{max}$ $v_{A2}=0$	$v_{B1}=0$ $v_{B2}=v_{mid}$	$v_{C1}=0$ $v_{C2}=-V_{dc}/2$

where, $v_{max}=\max(v_A, v_B, v_C)$, $v_{mid}=\text{mid}(v_A, v_B, v_C)$, $v_{min}=\min(v_A, v_B, v_C)$. According to the switching sequence of dual-inverter, the reference voltages of inverters 1 and 2 can be obtained as

$$\begin{cases} v_{A1}=(T_0/6+T_1/4+T_2/4)\,V_{dc}/T_s \\ v_{A2}=-(T_0/6)\,V_{dc}/T_s \\ v_{B1}=(T_0/6+T_2/4)\,V_{dc}/T_s \\ v_{B2}=-(T_0/6+T_1/4)\,V_{dc}/T_s \\ v_{C1}=(T_0/6)\,V_{dc}/T_s \\ v_{C2}=-(T_0/6+T_1/4+T_2/4)\,V_{dc}/T_s \end{cases}. \quad (4)$$

Substituting (3) into (4), the final expression of the reference voltage for dual-inverter can be determined, as given in Table I. The expression where the reference vector locates in other regions can also be given in Table I. The PWM signal can be obtained by comparing the reference voltage with the carrier. Switching sequences of modes II–V are shown in Fig. 7(b), (c), (d), and (e). Expression of the reference voltage for modes II–V can be obtained in the same manner, also given in Table I.

There are three issues need to be clarified.

1) For mode III, the switching sequence of inverter 1 is $\boldsymbol{V}_1\rightarrow\boldsymbol{V}_2\rightarrow\boldsymbol{V}_7\rightarrow\boldsymbol{V}_2\rightarrow\boldsymbol{V}_1$ when $\boldsymbol{V}_{ref}$ is located in region 5. The switching sequence of inverter 2 is $\boldsymbol{U}_0\rightarrow\boldsymbol{U}_5\rightarrow\boldsymbol{U}_4\rightarrow\boldsymbol{U}_5\rightarrow\boldsymbol{U}_0$, as shown in Fig. 8. It is necessary to shift the carrier of inverter 2 by π. The same process is required

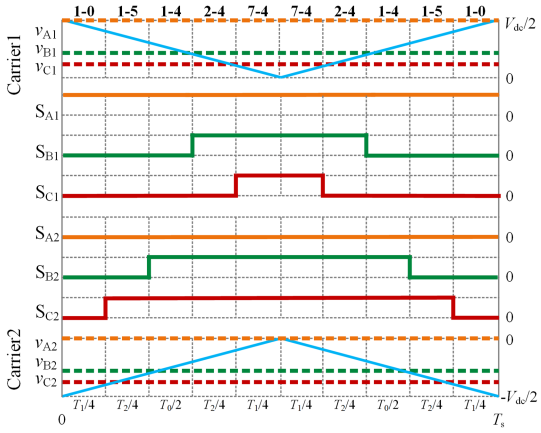

Fig. 8. Switching sequence of dual-inverter for mode III in region 5 of sector Z_I.

when $\boldsymbol{V}_{\text{ref}}$ is located in region 6. The dwell time T_0, T_1, and T_2 of basic vectors (including redundant vectors) are as follow:

$$\begin{cases} T_0 = -T_s v_{\min}/(V_{dc}/2) \\ T_1 = T_s\,(v_{\text{mid}} - v_{\min})/(V_{dc}/2)\ . \\ T_2 = T_s\,[1 + v_{\min}/(V_{dc}/2)] \end{cases} \tag{5}$$

According to the switching sequence of dual-inverter, the reference voltages of inverters 1 & 2 can be obtained as

$$\begin{cases} v_{A1} = V_{dc}/2 \\ v_{A2} = 0 \\ v_{B1} = (T_1/4 + T_2/4)\,V_{dc}/T_s \\ v_{B2} = (T_1/4 + T_2/4)\,V_{dc}/T_s - V_{dc}/2 \\ v_{C1} = (T_1/4)\,V_{dc}/T_s \\ v_{C2} = (T_1/4)\,V_{dc}/T_s - V_{dc}/2 \end{cases}. \tag{6}$$

The final expression of the reference voltage for dual-inverter are given in Table I.

2) For mode II, inverter 1 adopts CPWM and inverter 2 uses DPWM. Thus, the number of switching action in each carrier period are different for the two inverters. CPWM and DPWM should be adopted alternately for both the two inverters in each fundamental period to balance the switching loss. Modes III–V should also be designed in the same manner.
3) For modes I and II, the switching sequence cannot be designed in regions 3–6 due to the limitation of redundant vectors. The modulation range of modes I and II is $m \in [0, 0.5]$.
4) When the reference vector is located in region 1 of sector Z_I, basic vectors used for the synthesis of reference vector of traditional PWM (TPWM) [20] shown in Fig. 5(a) and modes I–V are shown in Fig. 9(a) and (b), respectively. As can be seen, the reference vector is synthesized by the nearest basic vectors for modes I–V. While for TPWM, non nearest vectors are used in the synthesization. The situation is the same when the reference vector falls in other regions and sectors.

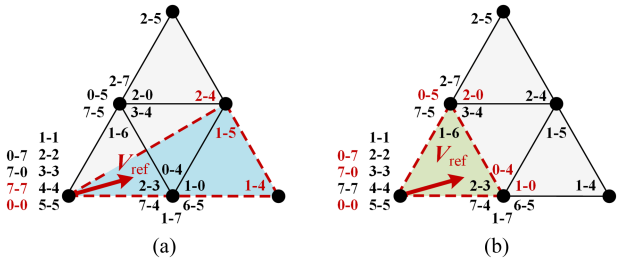

Fig. 9. Basic vectors used to synthesis the reference vector for modes I–V. (a) Traditional PWM. (b) Modes I–V.

TABLE II
PARAMETERS OF THE EXPERIMENTAL PLATFORM

Parameters	Unit	Value
DC-Bus Voltage V_{dc}	V	180
d/q Axis Inductance L_d / L_q	mH	2.415
Stator Resistance R_s	Ω	0.735
Rated Power P_e	kW	4.3
Rated Speed n_r	r/min	1500
Rated Torque T_e	N·m	27
Permanent Magnet Flux Linkage ψ	Wb	0.39
Carrier Frequency f_c	Hz	5000

Fig. 10 shows the control diagram of dual-inverter fed OW -PMSM. $i_d = 0$ control algorithm is used in this article because the OW-PMSM is surface-mounted. The implementation of the proposed multimode CBPWM strategy can be divided into the following steps.

1) *Modulation Mode Selection:* the appropriate modulation mode (modes I–V) is selected according to the modulation index m and the carrier frequency f_c.
2) *Reference Voltage Calculation:* the reference voltages v_{x1} and v_{x2} of inverters 1 and 2 are calculated according to Table I.
3) *PWM Generation:* PWM signals of each power switch can be obtained by comparing the reference voltage with carriers.

IV. ANALYSIS OF EXPERIMENTAL RESULTS

In order to verify the feasibility and effectiveness of the proposed multimode CBPWM strategy, an experimental platform of dual-inverter fed OW-PMSM with isolated dc sources is established, as shown in Fig. 11. An Opal-RT Simulator OP5700 is used as the controller, and Imperix SiC power module PEB8024 is used to compose dual-inverter. Parameters of the experimental platform are given in Table II. The output performance and switching loss of the proposed multimode PWM strategy are compared with that of TPWM.

Figs. 12 and 13 show reference voltages v_{A1}/v_{A2} and the PWM signals $S_{A1}\sim S_{C1}/S_{A2}\sim S_{C2}$ of the proposed multimode PWM strategy (modes I–V) and TPWM under the condition of $m = 0.5$ ($n = 640$ r/min, $T_L = 9$ N·m) and $m = 0.8$ ($n = 1100$ r/min, $T_L = 9$ N·m), respectively. As can be seen, there is no clamped leg at any instant for TPWM and mode I. However,

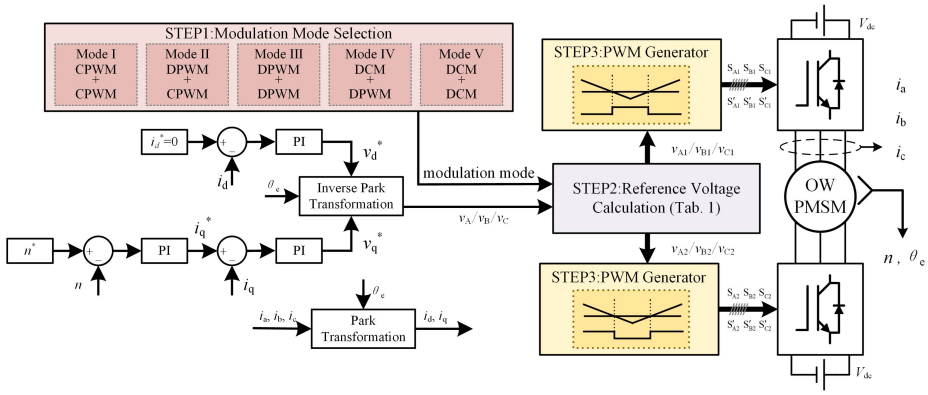

Fig. 10. Block diagram of the proposed multimode carrier-based PWM strategy.

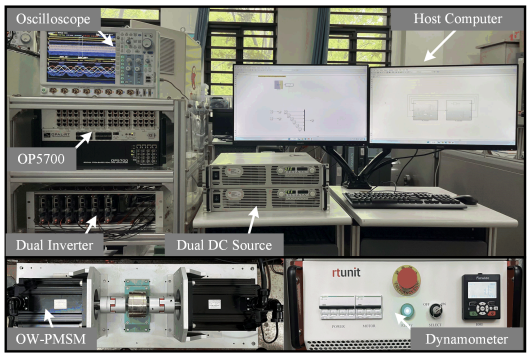

Fig. 11. Experimental platform of dual-inverter fed OW-PMSM with isolated dc sources.

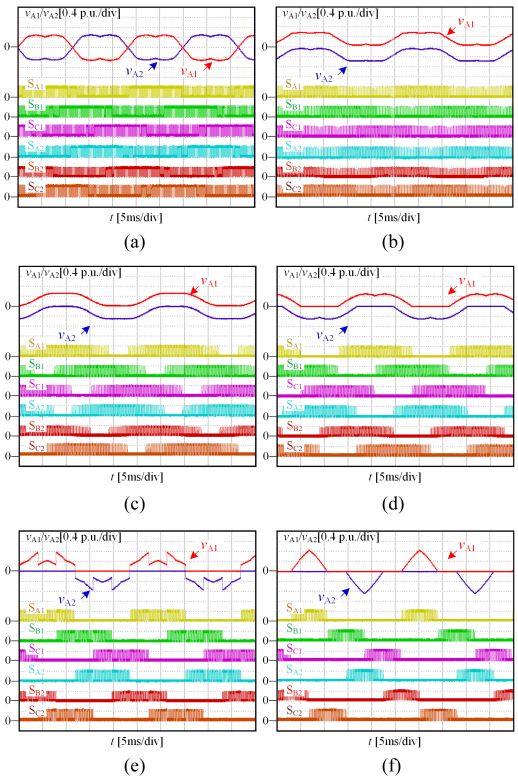

Fig. 12. Waveforms of reference voltage v_{A1}/v_{A2} and PWM signals of the upper leg in condition of $m = 0.5$. (a) TPWM. (b) Mode I. (c) Mode II. (d) Mode III. (e) Mode IV. (f) Mode V.

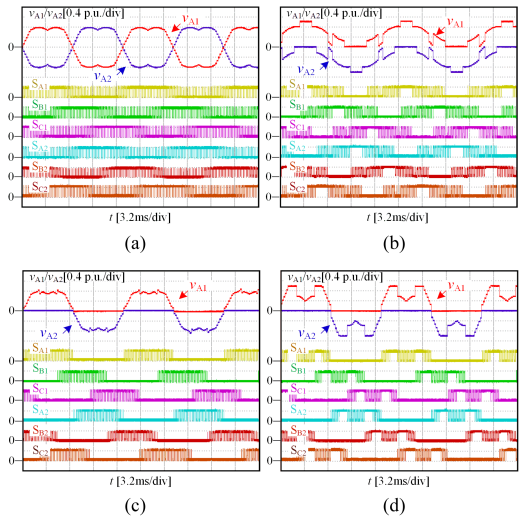

Fig. 13. Waveforms of reference voltage v_{A1}/v_{A2} and PWM signals of the upper leg in condition of $m = 0.8$. (a) TPWM. (b) Mode III. (c) Mode IV. (d) Mode V.

the number of clamped legs is increased from 1 to 4 for modes II–V, and the switching frequency of dual-inverter is reduced in turn. It is worth to be mentioned that although there are clamping intervals in the reference voltage of modes II–V, the clamping modes do not belong to DPWM0∼DPWM3.

Figs. 14 and 15 show the phase voltage v_A, line voltage v_{AB}, output current i_A and its harmonic spectrum of the proposed multimode PWM strategy (modes I–V) and TPWM under the condition of $m = 0.5$ and $m = 0.8$, respectively.

The total harmonic distortion of output current (I_{THD}) is defined as

$$I_{THD} = \frac{\sqrt{\sum_{n=2}^{\infty} I_n^2}}{I_1}. \tag{7}$$

From Figs. 14 and 15, it can be seen that common-mode components always exist in the phase voltage for both TPWM and the proposed multimode PWM strategy. As can be seen from the amplified waveforms, when $m = 0.5$, the output current ripple for modes I–V is significantly smaller than that of TPWM. The number of switching action for mode I is same as TPWM,

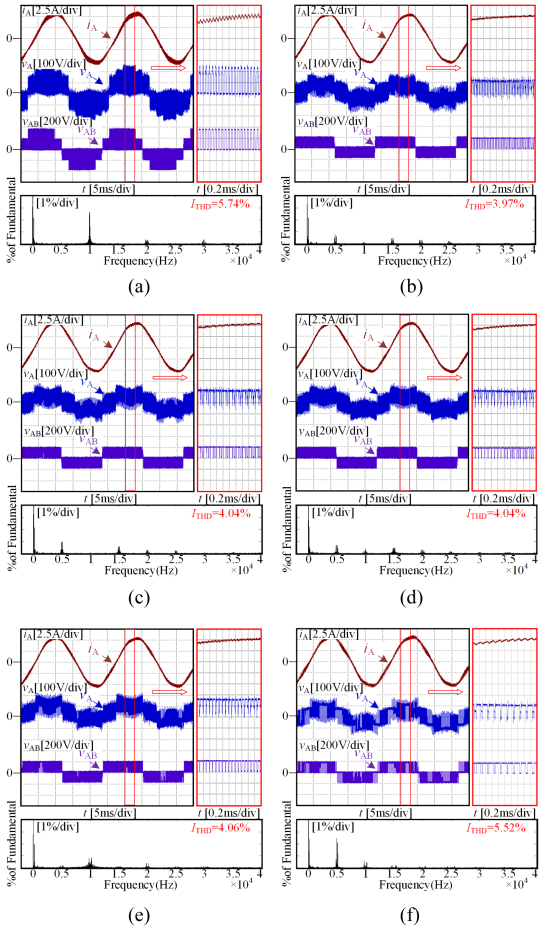

Fig. 14. Waveforms of output current i_{A}, phase voltage v_{A} and line voltage v_{AB} in condition of $m = 0.5$. (a) TPWM. (b) Mode I. (c) Mode II. (d) Mode III. (e) Mode IV. (f) Mode V.

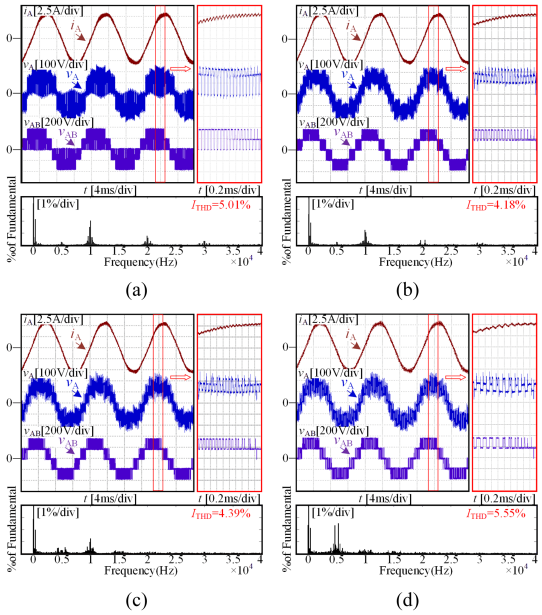

Fig. 15. Waveforms of output current i_A, phase voltage v_A and line voltage v_{AB} in condition of $m = 0.8$. (a) TPWM. (b) Mode III. (c) Mode IV. (d) Mode V.

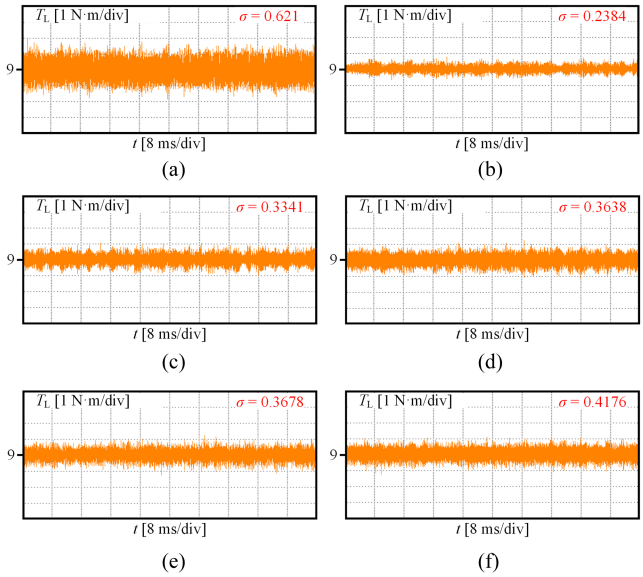

Fig. 16. Waveforms of T_{L} in the condition of $m = 0.5$. (a) Traditional PWM. (b) Mode I. (c) Mode II. (d) Mode III. (e) Mode IV. (f) Mode V.

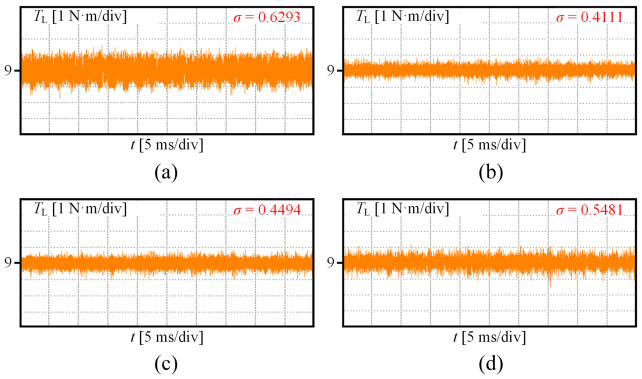

Fig. 17. Waveforms of T_{L} in the condition of $m = 0.8$. (a) Traditional PWM. (b) Mode III. (c) Mode IV. (d) Mode V.

while I_{THD} decreases from 5.74% to 3.97%. With the switching of modulation mode from mode II to mode V, I_{THD} gradually increases from 4.04% to 5.52% with the decrease of switching actions. When $m = 0.8$, I_{THD} is 5.01% with the adoption of TPWM. I_{THD} is 4.18% and 4.39% for modes III and mode IV, respectively, which is still lower than TPWM. I_{THD} is 5.55% with the adoption of mode V, which is slightly higher than TPWM. However, the switching frequency of the dual-inverter is reduced by 2/3.

For $m = 0.5$ and $m = 0.8$, the load torque T_{L} of TPWM and modes I–V are measured and shown in Figs. 16 and 17. The standard deviation σ is also calculated for each condition to characterize the smoothness of the torque. For $m = 0.5$, the torque ripple of modes I–V is clearly lower than that of TPWM. The torque ripple of mode I is the lowest. The torque ripple of modes II–IV are almost the same. For $m = 0.8$, the torque ripple of modes III–V are still significantly lower than that of TPWM. Mode V performs similarly to TPWM under this condition.

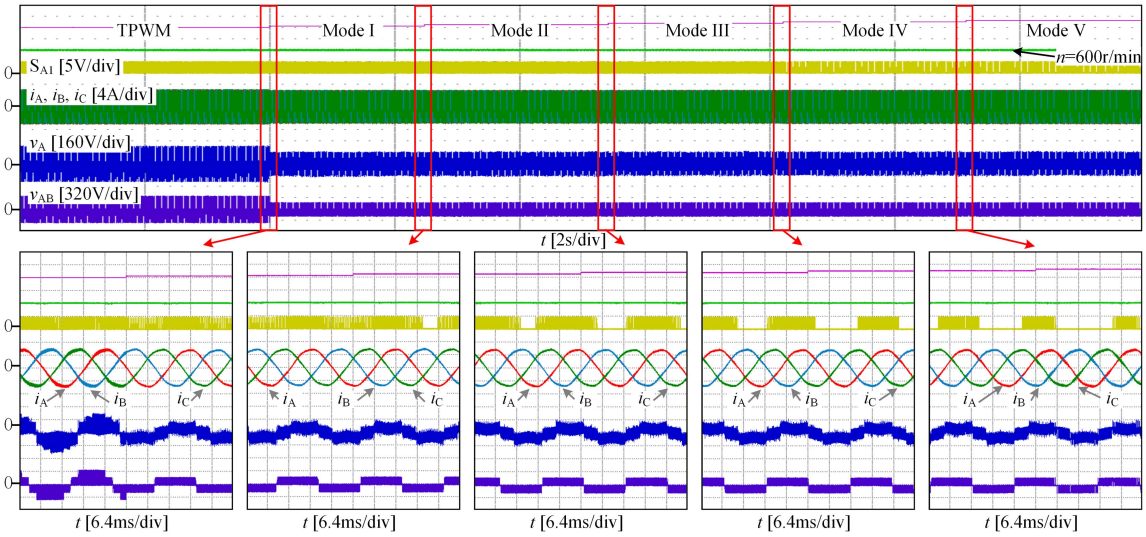

Fig. 18. Switching process of different modulation modes.

TABLE III
PERFORMANCE COMPARISON OF TPWM AND THE PROPOSED STRATEGY

Modulation Mode	Number of switching actions	Inverter efficiency (%)	I_{THD}(%)
TPWM(m=0.5)	6	95.873	5.74
Model I(m=0.5)	6	95.925	3.97
Model II(m=0.5)	5	96.412	4.04
Model III(m=0.5)	4	96.602	4.04
Model IV(m=0.5)	3	96.487	4.06
Model V(m=0.5)	2	97.809	5.52
TPWM(m=0.8)	6	97.714	5.01
Model III(m=0.8)	4	97.973	4.18
Model IV(m=0.8)	3	98.003	4.39
Model V(m=0.8)	2	98.288	5.55

Fig. 18 shows speed n of OW-PMSM, PWM signal S_{A1}, phase voltage v_A, line voltage v_{AB}, and three-phase current $i_A/i_B/i_C$ during the switching process from mode I to mode V under the condition of $n = 600$ r/min and $T_L = 9$ N·m. It can be seen that the motor speed is stabilized at 600 r/min before and after the switching of different modulation modes. It verifies that the proposed multimode modulation strategy can realize smooth switching between different modulation modes.

Table III gives the operating efficiency of the dual-inverter measured by a power analyzer under the condition of $m = 0.5$ and $m = 0.8$. For $m = 0.5$, the operating efficiency of TPWM and mode I are approximately the same. While for modes II–V, the operating efficiency is gradually increased with the decrease of switching actions in each carrier period. And the same conclusion can be obtained in condition of $m = 0.8$.

The variation of I_{THD} against m for TPWM and modes I–V is shown in Fig. 19. I_{THD} of mode I is the lowest when $m < 0.5$. I_{THD} decreases by nearly 30% compared with TPWM. In conditions of modes II–IV, I_{THD} is also lower than TPWM. While for mode V, I_{THD} is slightly higher than TPWM. When $0.5 < m < 0.7$, I_{THD} of modes III and IV are lower than TPWM, and there is not significant difference between these two modes.

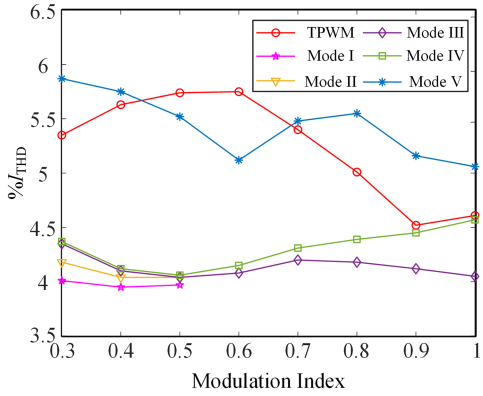

Fig. 19. Variation of I_{THD} against m for TPWM and modes I–V.

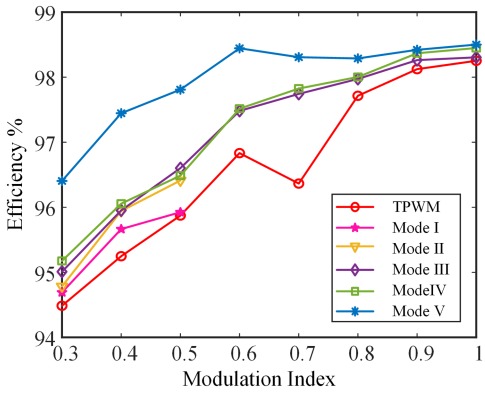

Fig. 20. Trends of the inverter operating efficiency with the variation of m.

When $m > 0.7$, I_{THD} of mode V is higher than TPWM. I_{THD} of the mode III and mode IV is lower than TPWM. I_{THD} of mode III is the lowest. In the whole modulation range, the waveform quality of the output current will be optimal if mode I is adopted when $m < 0.5$ and mode III is used when $m > 0.5$.

Fig. 20 shows the variation of operating efficiency in terms of modulation index. The efficiency of TPWM is relatively lower

in the whole modulation index range. For $0 < m < 0.5$, the efficiency is essentially the same under TPWM and mode I. The efficiency of modes II–IV is essentially the same but higher than TPWM, while the efficiency of mode V is significantly higher than modes II–IV. For $0.5 < m < 1$, the efficiency of mode V is still higher than other Modes and TPWM.

The versatility of the proposed multimode modulation strategy is discussed as follows.

1) The proposed multimode modulation strategy can be applied to dual neutral-point clamped three-level inverters. When the two inverters on both sides of the motor can output more voltage levels, more modulation modes can be designed.
2) If the voltage of the two isolated dc sources is not equal, the number of redundant voltage vectors in the space vector diagram will be reduced. Therefore, the reference vector could not be synthesized by the nearest basic vectors. The implementation of the multimode modulation strategy will be constrained.

V. Conclusion

A multimode carrier-based modulation strategy is proposed for dual-inverter fed OW-PMSM with isolated dc sources. Compared with traditional modulation methods, the proposed strategy has the following advantages.

1) Redundant switching states of dual-inverter is fully utilized. The reference voltage is always synthesized by the nearest switching state. the output waveform quality of dual-inverter is effectively improved.
2) Five modulation modes of dual-inverter are designed by the flexibly combination of CPWM, DPWM and DCM. Thus, the number of switching actions of dual-inverter can be changed from 2 to 6 in each carrier period.
3) The output performance and efficiency of OW-PMSM system can be improved under different working conditions by the use of different modulation modes.

References

[1] Z. Huang, T. Yang, P. Giangrande, M. Galea, and P. Wheeler, "Technical review of dual inverter topologies for more electric aircraft applications," *IEEE Trans. Transp. Electrific.*, vol. 8, no. 2, pp. 1966–1980, Jun. 2022.

[2] G. Zhang, Z. Zhou, T. Shi, and C. Xia, "An improved multimode synchronized space vector modulation strategy for high-power medium-voltage three-level inverter," *IEEE Trans. Power Electron.*, vol. 36, no. 4, pp. 4686–4696, Apr. 2021.

[3] H. Matsumori, Y. Maeda, T. Kosaka, N. Matsui, and S. Saha, "Dual inverter-fed open winding IPMSM drive system for high-power premium class EV," *IEEE Trans. Ind. Appl.*, vol. 59, no. 2, pp. 2069–2080, Mar./Apr. 2023.

[4] X. Xu et al., "Modulation and voltage balancing control of dual five-level ANPC inverter for ship electric propulsion systems," *Chin. J. Elect. Eng.*, vol. 7, no. 4, pp. 78–92, Dec. 2021.

[5] J. Wei, Q. Deng, B. Zhou, M. Shi, and Y. Liu, "The control strategy of open-winding permanent magnet starter-generator with inverter-rectifier topology," *IEEE Trans. Ind. Inform.*, vol. 9, no. 2, pp. 983–991, May 2013.

[6] Q. An, J. Liu, Z. Peng, L. Sun, and L. Sun, "Dual-space vector control of open-end winding permanent magnet synchronous motor drive fed by dual inverter," *IEEE Trans. Power Electron.*, vol. 31, no. 12, pp. 8329–8342, Dec. 2016.

[7] S. Chowdhury, P. W. Wheeler, C. Patel, and C. Gerada, "A multilevel converter with a floating bridge for open-end winding motor drive applications," *IEEE Trans. Ind. Electron.*, vol. 63, no. 9, pp. 5366–5375, Sep. 2016.

[8] Z. Huang, T. Yang, P. Giangrande, S. Chowdhury, M. Galea, and P. Wheeler, "An active modulation scheme to boost voltage utilization of the dual converter with a floating bridge," *IEEE Trans. Ind. Electron.*, vol. 66, no. 7, pp. 5623–5633, Jul. 2019.

[9] S. Srinivas and K. Ramachandra Sekhar, "Theoretical and experimental analysis for current in a dual-inverter-fed open-end winding induction motor drive with reduced switching PWM," *IEEE Trans. Ind. Electron.*, vol. 60, no. 10, pp. 4318–4328, Oct. 2013.

[10] R. Baranwal, K. Basu, and N. Mohan, "Carrier-based implementation of SVPWM for dual two-level VSI and dual matrix converter with zero common-mode voltage," *IEEE Trans. Power Electron.*, vol. 30, no. 3, pp. 1471–1487, Mar. 2015.

[11] W. Hu, C. Ruan, H. Nian, and D. Sun, "Zero-sequence current suppression strategy with common-mode voltage control for open-end winding PMSM drives with common DC bus," *IEEE Trans. Ind. Electron.*, vol. 68, no. 6, pp. 4691–4702, Jun. 2021.

[12] W. Hu, H. Nian, and D. Sun, "Zero-sequence current suppression strategy with reduced switching frequency for open-end winding PMSM drives with common DC bus," *IEEE Trans. Ind. Electron.*, vol. 66, no. 10, pp. 7613–7623, Oct. 2019.

[13] J. Ewanchuk, J. Salmon, and C. Chapelsky, "A method for supply voltage boosting in an open-ended induction machine using a dual inverter system with a floating capacitor bridge," *IEEE Trans. Power Electron.*, vol. 28, no. 3, pp. 1348–1357, Mar. 2013.

[14] C. Perera, G. J. Kish, and J. Salmon, "Decoupled floating capacitor voltage control of a dual inverter drive for an open-ended winding induction motor," *IEEE Trans. Power Electron.*, vol. 35, no. 7, pp. 7305–7316, Jul. 2020.

[15] Z. Huang, T. Yang, P. Giangrande, S. Chowdhury, M. Galea, and P. Wheeler, "Enhanced performance of dual inverter with a floating capacitor for motor drive applications," *IEEE Trans. Power Electron.*, vol. 36, no. 6, pp. 6903–6916, Jun. 2021.

[16] A. D. Kiadehi, K. E. K. Drissi, and C. Pasquier, "Voltage THD reduction for dual-inverter fed open-end load with isolated DC sources," *IEEE Trans. Ind. Electron.*, vol. 64, no. 3, pp. 2102–2111, Mar. 2017.

[17] W. Hu, C. Ruan, H. Nian, and D. Sun, "An improved modulation technique with minimum switching actions within one PWM cycle for open-end winding PMSM system with isolated DC bus," *IEEE Trans. Ind. Electron.*, vol. 67, no. 5, pp. 4259–4264, May 2020.

[18] G. Nadh and A. Rahul S, "Clamping modulation scheme for low-speed operation of three-level inverter fed induction motor drive with reduced CMV," *IEEE Trans. Ind. Appl.*, vol. 58, no. 6, pp. 7336–7345, Nov./Dec. 2022.

[19] T.-H. Kim, J.-H. Lee, B.-R. Yoon, and J.-S. Lee, "Clamping modulation technique for balancing power losses of dual inverter with isolated DC bus," *IEEE Access*, vol. 11, pp. 41868–41879, 2023.

[20] L. Xu, Z. Q. Zhu, and L. Yan, "Low switching frequency SPWM strategies for open-winding machine with low current harmonics," *IEEE Trans. Ind. Appl.*, vol. 58, no. 2, pp. 2042–2054, Mar./Apr. 2022.

[21] M. Zerdani, S. A. E. M. Ardjoun, H. Chafouk, and M. Denaï, "Experimental investigation of decoupled discontinuous PWM strategies in open-end winding induction motor supplied by a common DC-link," *IEEE J. Emerg. Sel. Topics Power Electron.*, vol. 11, no. 3, pp. 3087–3096, Jun., 2023.

[22] M. H. V. Reddy, T. B. Reddy, B. R. Reddy, and M. S. Kalavathi, "Discontinuous PWM technique for the asymmetrical dual inverter configuration to eliminate the overcharging of DC-link capacitor," *IEEE Trans. Ind. Electron.*, vol. 65, no. 1, pp. 156–166, Jan., 2018.

[23] K. R. Sekhar and S. Srinivas, "Discontinuous decoupled PWMs for reduced current ripple in a dual two-level inverter fed open-end winding induction motor drive," *IEEE Trans. Power Electron.*, vol. 28, no. 5, pp. 2493–2502, May 2013.

[24] H. Matsumori, T. Kosaka, N. Matsui, and S. Saha, "Alternative PWM switching strategy implementation for a dual inverter fed open winding motor drive system for an electric vehicle application," *IEEE Trans. Ind. Appl.*, vol. 59, no. 5, pp. 5957–5970, Sep./Oct. 2023.

[25] M. Pathmanathan, S. Semsar, C. Viana, and P. W. Lehn, "Power sharing control algorithm for direct integration of fuel cells in a dual-inverter electric vehicle drivetrain," *IEEE Trans. Transp. Electrific.*, vol. 8, no. 2, pp. 2490–2500, Jun. 2022.

[26] H. Matsumori, T. Kosaka, N. Matsui, and S. Saha, "Inverter power device fault detection and fail safe action strategy for electric vehicle with a dual inverter fed open winding motor," *IEEE Trans. Ind. Appl.*, vol. 59, no. 3, pp. 3875–3888, May–Jun. 2023.

Xin Gu (Member, IEEE) was born in Tianjin, China, in 1980. He received the B.S., M.S., and Ph.D. degrees from Tianjin University, Tianjin, China, in 2003, 2006, and 2010, respectively, all in electrical engineering.

He is currently a professor with the School of Electrical Engineering, and with the National Local Joint Engineering Research Center of Electrical System Design and Manufacturing. He is also the Deputy Director with Electrical Machine System Research Institute, Tiangong University, Tianjin, China. His research interests include permanent magnet synchronous machines, power electronic converters and their control systems.

Yufei Liu (Student Member, IEEE) was born in Tianjin, China, in 2000. He received the B.S. degree in electrical engineering in 2022 from Tiangong University, Tianjin, China, where he is currently working toward the Ph.D. degree in control science and engineering with the School of Control Science and Engineering.

His research interests include electrical machines, multilevel converters, and their control systems.

Guozheng Zhang (Member, IEEE) was born in Datong, China, in 1985. He received the B.S. degree from Tianjin University, Tianjin, China, in 2008, the M. S. degree from Tianjin University of Science and Technology, Tianjin, China, in 2011, and the Ph.D. degree from Tianjin University, Tianjin, China, in 2017, all in electrical engineering.

He is currently an Associate Professor with the School of Electrical Engineering, Tiangong University, Tianjin, China, and also with the National Local Joint Engineering Research Center of Electrical System Design and Manufacturing. His research interests include electrical machines, multilevel converters and their control systems.

Yanfei Cao (Member, IEEE) was born in Hebei, China, in 1989. She received the M.S. and Ph.D. degrees in control science and engineering from Tianjin University, Tianjin, China, in 2019.

From 2019 to 2021, she was a Postdoctoral Researcher with the College of Electrical Engineering, Zhejiang University, Zhejiang, China. She is currently an Associate Researcher with the College of Electrical Engineering, Zhejiang University. Her research interests include electrical machines, motor drives, and power electronics.

Changliang Xia (Senior Member, IEEE) was born in Tianjin, China, in 1968. He received the B.S. degree from Tianjin University, Tianjin, China, in 1990, and the M.S. and Ph.D. degrees from Zhejiang University, Hangzhou, China, in 1993 and 1995, respectively, all in electrical engineering.

He was elected Academician of the Chinese Academy of Engineering in 2017. He is a Researcher with the Zhejiang University Advanced Electrical Equipment Innovation Center, Hangzhou, China, and also a Professor with Tiangong University, Tianjin, China. He is currently the Qiushi Chair Professor with Zhejiang University. His research interests include electrical machines, power electronics, and their control systems.